Cytosolic ribosomes on the surface of mitochondria

Vicki A. M. Gold*[♯1,2], Piotr Chroscicki*[3], Piotr Bragoszewski[3] & Agnieszka Chacinska[♯3,4]

[1] Department of Structural Biology, Max Planck Institute of Biophysics, Max-von-Laue Str. 3, 60438 Frankfurt am Main, Germany

[2] Living Systems Institute, University of Exeter, Stocker Road, EX4 4QD, United Kingdom

[3] The International Institute of Molecular and Cell Biology, Ks. Trojdena 4, 02-109 Warsaw, Poland

[4] Centre of New Technologies, Warsaw University, Banacha 2c, 02-097 Warsaw, Poland

Vicki Gold: vicki.gold@biophys.mpg.de

Agnieszka Chacinska: achacinska@iimcb.gov.pl

Footnotes:

*equal first author contribution

[♯]corresponding authors

Abstract

By electron cryo-tomography and subtomogram averaging, translation-arrested ribosomes were used to depict the clustered organisation of the TOM complex on the surface of mitochondria, corroborating earlier reports of localized translation. Ribosomes were shown to interact specifically with the TOM complex and nascent chain binding was crucial for ribosome recruitment and stabilization. Ribosomes were bound to the membrane in discrete clusters, often in the vicinity of the crista junctions. This interaction highlights how protein synthesis may be coupled with transport, and the importance of spatial organization for efficient mitochondrial protein import.

Keywords: Electron cryo-tomography/ mitochondrial protein import/ TOM complex/ ribosomes/ translation

Introduction

Historically, cytosolic ribosomes were thought to exist in two main pools, a free solution state and a endoplasmic reticulum (ER) membrane-bound state [1, 2], both recently visualized *in situ* [3]. The membrane-bound ribosomes are engaged in a well-orchestrated process, in which protein synthesis is mechanistically coupled to protein translocation into the ER. This so called co-translational mode of transport utilizes mechanisms that lead to translational stalling and precise positioning of the ribosomes at the ER membrane translocon, the Sec complex [4-8].

Mitochondria constitute an important bioenergetic, metabolic and signaling hub, and the biogenesis of mitochondrial proteins is an important factor that determines the organelle's function. The mitochondrial proteome of the yeast *Saccharomyces cerevisiae* is composed of approximately 1000 proteins [9]. Almost all of them (99%) are nuclear encoded, despite the presence of mitochondrial DNA. Mitochondria-destined precursor proteins are synthesised on cytosolic ribosomes and are actively imported through the **T**ranslocase of the **O**uter **M**embrane (TOM) complex. TOM forms a common entry gate for mitochondrial precursor proteins that are subsequently targeted to various mitochondrial locations [10-16]. Mitochondria have a double-membrane structure, thus proteins destined for the mitochondrial matrix or inner membrane are subsequently transported through one of two protein translocases of the inner membrane. Proteins that possess positively charged N-terminal presequences are substrates for the **T**ranslocase of the **I**nner **M**embrane (TIM23) complex [10-16].

For decades, it has been known that precursor proteins can be imported into mitochondria post-translationally, after completion of their synthesis in the cytosol or

in vitro in a ribosome free system [12, 17-19]. Meanwhile, cytosolic ribosomes were detected in the vicinity of mitochondria by electron microscopy (EM), suggesting a role for co-translational import [20, 21]. Additionally, various independent approaches have shown an enrichment of mRNAs encoding mitochondrial proteins, either on the mitochondrial surface or in close proximity, both in yeast [22-27] and human cells [28, 29]. Their association was dependent on COP1- mediated targeting [30] and involved the outer membrane-associated protein Puf3, which binds 3' non-coding sequences of mRNAs [31, 32]. Mitochondrial surface-localized mRNA molecules were also found to be active as templates for protein synthesis [27]. The mechanism of **R**ibosome-**N**ascent **C**hain **C**omplex (RNC) recruitment to mitochondria was also investigated by a *de novo* ribosome binding assay [33-37]. In summary, there is a great deal of data in support of localized synthesis of proteins at the mitochondrial outer membrane, yet the co-localization of cytosolic ribosomes with TOM complex has never been shown to date.

Electron cryo-tomography (cryoET) is a technique by which proteins or complexes may be studied *in situ*. Samples are preserved by cryo-fixation, imaged in the electron microscope, and structures can be determined by subtomogram averaging (StA) [38]. The post-translational route for protein import into mitochondria was previously studied by this method, revealing details of TOM-TIM23 supercomplex localization and distribution [39]. In this work, we isolated native mitochondria with bound ribosomes, confirming earlier reports of localized translation on the mitochondrial surface. Ribosome numbers were low, thus we devised a method to isolate sufficiently high numbers of **M**itochondria with **A**ssociated **R**ibosomes (MAR) by translation arrest with cycloheximide (CHX) treatment. Samples were characterized biochemically and imaged using cryoET and StA. This demonstrated that a specific interaction between ribosomes and the TOM complex occurs, and nascent chain binding is crucial for ribosome

recruitment and stabilization on the mitochondrial outer membrane. Ribosomes, which mark the position of TOM complexes, are organized on the mitochondrial surface in discrete clusters, often within the vicinity of the mitochondrial crista junctions (CJs), providing a long awaited view of mitochondrial bound cytosolic ribosomes.

Results

Cytosolic ribosomes co-purify with mitochondria and can be stabilized on the outer membrane

In standard preparations of isolated yeast mitochondria, cytosolic ribosomes are not observed bound to the outer membrane by cryoET (Fig 1A & D) [39]. We first investigated if mitochondria-bound RNCs could be enriched with magnesium acetate ($Mg(OAc)_2$), as Mg^{2+} ions are essential for ribosome and RNC stabilization. In mitochondrial preparations isolated in the presence of $Mg(OAc)_2$, we were able to clearly identify ~3 ribosomes (per μm^2 mitochondrion surface area) bound to mitochondria on average (Fig 1A, E - H & Fig EV1A), confirming the stabilizing effect of Mg^{2+}. As the number of bound ribosomes was too low for quantitative statistical analysis of protein import, we investigated further conditions for ribosome stabilization, such as CHX treatment of the cells and CHX inclusion in the buffers for mitochondrial isolation. CHX is known to block the translocation step of elongation, thus stabilizing RNCs [40-42]. Now ~45 ribosomes (per μm^2 mitochondrion surface area) could be clearly identified on the mitochondrial membrane, a 15-fold increase (Fig 1A, I & Fig EV1A). The Mg^{2+} and CHX-treated mitochondria are subsequently referred to as MAR. The steady-state protein levels of isolated control and MAR samples were analyzed to confirm observations made by cryoET (Fig 1B). Accordingly, protein markers of both the 60S (uL22 and uL4) and the 40S ribosome (uS4) were significantly increased in the MAR

sample compared to the control. Interestingly, the MAR sample also contained an increased level of Egd1, which is a β subunit of the NAC complex [43-45]. Marker proteins for mitochondria (Tom40, Tom20, Mia40, Cyc3), cytosol (Pgk1) and ER (Sec61, Pdi1) remained in equal amounts between control and MAR samples (Fig 1B).

Mitochondria exist in a dynamic network and interact closely with other organelles in the cell, most notably the ER [46]. Thus, mitochondria isolated by differential centrifugation inevitably co-purify with ER-membranes of similar density. Consequently, CHX treatment also had the effect of increasing the overall level of ribosomes, which were observed either bound to ER-membranes, or were free in solution (Fig 1J). These background ribosomes were often found in close proximity to mitochondria and made accurate statistical and structural analysis extremely challenging. Therefore, an iodixanol gradient purification step [39] was included to remove soluble material and a proportion of rough ER membranes, as visualized by western blot analysis (Fig 1C). Mitochondrial marker proteins (Tom70, Ccp1, Cox12) were mostly enriched in 15-21% fractions, similar to the ribosomal marker proteins uS4 and uL22. These three fractions were pooled for further analysis by cryoET. The purification step removed a portion of free cytosolic ribosomes and rough ER membranes (Fig 1C, K & Fig EV1B). The purification step did not adversely affect the number of ribosomes bound stably to the outer membranes of mitochondria (Fig 1A & Fig EV1A).

Ribosome binding to mitochondria is dependent on protein import and involves the TOM complex

The TOM complex is the exclusive entry gate for imported mitochondrial proteins. Therefore, to test the specificity of ribosomes binding to mitochondria, we assessed the cytosolic ribosome interaction with the TOM complex in MAR samples. Affinity

purification of the TOM complex, via its Histidine10-tagged core protein Tom22, demonstrated that the ribosomal protein marker uL22 and the ribosome-localized Hsp70 family chaperone Ssb1 could be co-purified (Fig 2A, lane 7). The ribosome-$Tom22_{HIS}$ interaction was lost when MAR samples were pretreated with EDTA (Fig 2A, lane 8), which leads to ribosome dissociation by depletion of Mg^{2+} ions. To confirm this result, the ribosome-TOM complex interaction was further investigated by an alternative approach. Affinity purification via HA-tagged Tom40, the TOM complex component that forms the central pore of the translocase, demonstrated the co-purification of ribosomal protein uL22 from MAR samples (Fig EV2A, lane 4). Similarly, uL22 and Ssb1 were eluted with $Tom40_{HA}$ when high molecular weight (HMW) membranes, that also contain mitochondrial membranes (Fig EV2B), were subjected to affinity purification (Fig 2B, lane 4).

The observed interaction of ribosomes with the TOM complex could be mediated by nascent chains of mitochondrial precursor proteins. To test this hypothesis, we analyzed ribosome association with mitochondria after dissipation of the electrochemical potential (-ΔΨ) of the mitochondrial inner membrane with carbonyl cyanide *m*-chlorophenyl hydrazone (CCCP), as precursors with N-terminal presequences and hydrophobic inner membrane proteins are known to require the –ΔΨ for their import [12, 13, 16]. We observed a reduction in the amount of ribosomes associated with mitochondria-enriched membranes in the samples treated with CCCP, as indicated by ribosome marker proteins (uS4, uL22 and Egd1) (Fig 2C). This reduction was dependent on the time of CCCP treatment (Fig 2C & D). It was shown previously that mitochondrial precursor proteins accumulate in the cytosol upon dissipation of the –ΔΨ [18, 47]. However, simultaneous treatment with CCCP and CHX did not reduce the amount of ribosomes in isolated MAR and HMW membrane samples (Fig EV2C & D,

lane 4). This may indicate that CCCP does not affect the localization of ribosomes that are already stably bound to mitochondria. We reasoned that ribosome-bound nascent chain import is involved in RNC binding to the mitochondrial outer membrane. Thus, the nascent chain release should cause a ribosome dissociation from mitochondria. Puromycin is a commonly used translation inhibitor that competes with aminoacetylated tRNA at the ribosomal A site, causing premature translation termination and polypeptide release [48]. However, the use of CHX during MAR isolation procedure blocks nascent chain puromycilation. CHX inhibits eEF2-mediated mRNA translocation showing a dominant effect over puromycin [42, 49]. For this reason we applied hydroxylamine (NH_2OH) as a nascent chain releasing agent [50, 51]. Hydroxylamine is a small compound that can reach the ribosomal active site and break the tRNA-peptide bond. To confirm hydroxylamine properties we took advantage of RNCs harboring the nascent chain for Tim9 (directed to the intermembrane space), which was lacking a stop codon [52, 53]. A radiolabeled nascent chain bound to ribosomes can be detected in a complex with tRNAs when analyzed by SDS-PAGE [52] (Fig. EV2E, lane 1). Incubation of RNCs containing Tim9 with hydroxylamine caused the aminolysis of tRNA-Tim9 complexes and formation of mature-size Tim9 protein (Fig EV2E, lane 2). Next, we tested the effect of hydroxylamine on MAR samples and found that ribosomes were dissociated from mitochondria upon treatment (Fig 2E, lane 2-5 & F, Fig EV2F lane 2-5 & G). As expected, puromycin was not effective due to prior use of CHX during MAR isolation (Fig 2E, lane 6). To further confirm that ribosomes dissociate from mitochondria upon nascent chain release, we subjected MAR samples preincubated with 1,5M hydroxylamine to centrifugation in an iodixanol gradient as before. The majority of ribosomal proteins (uS4, uL22) and ribosome associated proteins (Ssb1) were now detected in lighter fractions, similar to the cytosolic protein Pgk1 (Fig EV2H). By cryoET, only 15 mitochondria-bound ribosomes (per μm^2

mitochondrion surface area) could be identified in hydroxylamine-treated and purified MAR samples, showing a 66% reduction compared to the untreated state (Fig EV2I). To exclude a negative effect of high hydroxylamine concentration on the ribosome 80S structure, we purified cytoplasmic ribosomes preincubated with 1.5 M hydroxylamine using the TAP-tagged large ribosomal subunit uL13a$_{TAP}$. The ribosomal proteins (uS4 and uL22) were detected in the eluate at the same level in the control as well as the hydroxylamine treated sample (Fig 2G, lanes 3 & 4). These results confirmed that nascent chain release from the ribosome by hydroxylamine treatment does not cause 80S ribosome disassembly. Interestingly, hydroxylamine caused dissociation of the Ssb1 protein from the ribosome (Fig 2G, lane 4). In line with our findings, previous reports showed that Ssb1 proteins interact only with active ribosomes, when the nascent chain is long enough to emerge from the exit tunnel [33, 44, 54]. To conclude, the binding of ribosomes to the mitochondrial surface was sensitive to hydroxylamine, which specifically removes nascent chains from the ribosome.

Mitochondrial-bound ribosomes are specifically oriented for protein import

To investigate the 3D localization of ribosomes bound to mitochondria, iodixanol purified MAR samples were investigated in detail by cryoET and StA (Fig 3). Two different populations of ribosomes could be clearly observed; the first was a distinct group located at the mitochondrial membrane (MAR-M, orange arrowheads in Fig 3A-C) and the second group was more peripherally associated (MAR-P, blue arrowheads in Fig 3A & C). In order to visualize ribosome distribution and their specific orientation with respect to the membrane, the MAR-M (1215 subvolumes) and MAR-P (419 subvolumes) structures were determined by StA (Fig 3D, E & Fig EV3). Placing the MAR-M and MAR-P structures back into the 3D volume revealed a number of interesting details. Firstly, both groups form discrete clusters on mitochondria (Fig 3F), in

agreement with previous data reporting on the distribution of proteins arrested through TOM-TIM23 supercomplexes [39]. Soluble MAR-P clusters are associated with a neighbouring MAR-M groups (Fig 3F). In general, polysomes form clusters that translate mRNA simultaneously and form highly flexible structures [55-57]. On this basis, we suggest that ribosomes in the MAR-P group are polysomes, attached to MAR-M ribosomes through mRNA molecules (Fig 3G).

In the MAR-M population, ribosomes were clearly specifically oriented with the polypeptide exit tunnel pointing towards the outer membrane for import, often observed within the vicinity of the CJs (Fig 3G, H). Ribosomes were also observed to group locally around a tubular section of one mitochondrion, which is possibly a fission constriction (Fig 3I-L) [58]. Interestingly, TOM-TIM23 arrested preproteins were previously found to cluster around a fusion septum [39], providing additional support for the idea that protein import sites occur at specific microdomains.

Using ribosomes to investigate clustering of the TOM complex

The ribosome provides an effective tool to mark the position of the TOM complex *in situ*. To investigate observed clustering of protein import sites on the mitochondrial surface in more detail, distance calculations were made between individual ribosomes and their closest neighbour using an established protocol [39]. This revealed that ~90% of TOM complexes exist in discrete clusters, marked by two or more ribosomes located <50 nm apart (Fig 4A). For statistical analysis of ribosome numbers, the absolute values of both MAR-M and MAR-P populations on individual mitochondria were correlated to the surface area of the outer membrane. This revealed a linear correlation for both populations, with an average value of 157 MAR-M (TOM complexes) and 84 MAR-P per μm^2 outer membrane surface respectively (Fig 4B). Many recent reports detail the

relationship between the import machinery and the CJ [52, 59-62]. To directly visualize the spatial relationship between the TOM complex and the CJ *in situ*, the distance between each MAR-R ribosome and its nearest CJ was calculated (Fig EV4). This was compared to previous data (now visualised differently) showing the distribution of saturated TOM-TIM23 supercomplexes (Fig 4C). This analysis revealed that whilst both TOM and TOM-TIM23 supercomplexes tend to cluster preferentially around CJs, the TOM complex distribution is significantly broader than that of TOM-TIM23 (Fig 4D). Additional statistical analyses were performed to investigate the distribution of cluster sizes. For both data sets, <15% of ribosomes existed as a single entity, and the major group size was between 2-5 ribosomes per cluster (Fig 4E & F). In the MAR-M population, ~5% of ribosomes existed in 'superclusters', defined as a group of >26 ribosomes. MAR-P clusters existed in groups of maximum 25 ribosomes, similar to that reported previously for cytosolic ribosomes observed in whole cells [56]; in this case 'superclusters' were not seen (Fig 4F).

Comparison to ribosome tethering to the ER

From the same samples that were used for cryoET of MAR-M and MAR-P, 230 **ER**-bound **R**ibosomes (ER-R) could also be identified for StA from the same tomograms (Fig 5A, B & Fig EV3). Visualization of the resulting average in the 3D volume also revealed discrete clusters on small vesicles (Fig 5C). However, as we only report on a small part of the ER-R population, detailed statistical analysis of clustering was not carried out. A small density could be observed to make a connection between ribosomes and the ER membrane (Fig 5D). By docking X-ray structures of yeast ribosomes [63] into the ER-R and MAR-M StA maps, the density was identified as rRNA expansion segment eS7^{L}a (Fig 5E). This is in agreement with previous reports of ER membrane-associated canine ribosomes [57]. Contra to the ER-R population, at this resolution eS7^{L}a is not seen to

connect to the mitochondrial membrane (Fig 5F). No density was observed for rRNA expansion segment eS27^{L} in either structure (Fig 5E & F), in line with previous reports of its extremely dynamic behavior [63].

The lack of protein or rRNA density between the ribosome and the mitochondrial membrane suggests that CHX-stabilized ribosomes could be tethered to the TOM complex by the polypeptide chain only. Analysis of the distances between MAR-M or ER-R populations and their corresponding membranes demonstrated the variability in tethering between the two groups. The average distance (measured from the base of the cleft between the 60S and 40S subunits to the membrane) was similar, at ~13 nm and ~ 12 nm respectively (Fig 5G & Fig EV5). The more notable difference was the variation in tethering distances, with variance calculated at 8.6 nm for MAR-M and 3.2 nm for ER-R populations respectively (Fig 5G, H & Fig EV5). With respect to tethering distances, the ER-R group displayed a clear narrow distribution, with ~70% of ribosomes within the range 10-14 nm from the membrane. The MAR-M group however displayed a much wider distribution, with only ~50% within the same range. A StA calculated for the MAR-M population that included only ribosomes located within the 10-14 nm range (240 particles, a similar number to that used in the ER-R average) did not result in additional information (data not shown). Due to the extremely low number of ribosomes bound in conditions without CHX stabilization, StA was not possible. Such a flexible mode of tethering agrees with the observation that the MAR-M population exhibits a significant degree of orientational flexibility with respect to the position of the polypeptide exit tunnel relative to the membrane (Fig 3H).

Discussion

Using cryoET, we were able to provide supportive evidence for the existence of co-translational import into isolated mitochondria. Using CHX-arrested RNCs bound to mitochondria, we performed StA and biochemical analyses to demonstrate that cytosolic ribosomes are localized at the mitochondrial outer membrane due to nascent chain import. This is based on several lines of evidence described as follows. Firstly, we were able to detect the ribosome-TOM complex interaction, which was reversible by induction of nascent chain release. CryoET and StA revealed two groups of associated ribosomes, a distinct population located at the mitochondrial membrane (MAR-M), and a second group of soluble polysomes (MAR-P). The MAR-M group was directionally oriented with the polypeptide exit tunnel pointing towards the membrane for import and was tethered through the TOM complex by the polypeptide chain. The ribosomes in the MAR-P population displayed more undefined orientations. In human cells, polysomes were found to exist in various conformations, ranging from unordered to helical, planar and spiral [56]. It is possible that organelle isolation and thus the absence of certain cytosolic factors could result in the predominantly undefined orientations described here.

The tethering distance between MAR-M and the mitochondrial membrane and ER-R and the ER membrane is 12-13 nm, but the variance is approximately 3-fold more (8.6 nm to 3.2 nm) for MAR-M. The larger variation in tethering distance is likely due to the flexibility and varying angle of attachment afforded by the connection made through a nascent polypeptide chain. Interestingly, dissipation of the membrane potential by the chemical uncoupler CCCP affected ribosome association with mitochondria only if CCCP treatment preceded the addition of CHX. This indicates that post lysis RNC recruitment to mitochondria had no significant effect on our results. These data do not exclude the presence of a specific mitochondrial receptor for ribosomes that may be critical for

specific earlier steps of import, such as binding and initiation. A connection is observed between ER-R and the membrane by eS7^{L}a, which is flexible in yeast as it is not stabilized by ribosomal proteins such as L28e, found in other species [63]. This could explain why eS7^{L}a appears to be partially twisted away in both structures, similar to that observed previously [4].

Here, we were able to locate 167 TOM complexes per μm^2 outer membrane surface, approximately 2-fold more than the 69 TOM-TIM23 import sites determined in the previous study [39]. This is in agreement with the fact that TOM is more abundant in mitochondria than TIM23 [64]. We also demonstrate that import through the TOM complex occurs in the vicinity of CJs, but this distribution is significantly broader than for arrested TOM-TIM23 supercomplexes. Our data therefore highlight key roles that the TIM23 complex may play in the mitochondrial organizing network. Both MAR-M and MAR-P were seen to associate with mitochondria in the form of clusters, also observed for proteins imported by the TOM-TIM23 route [39]. Import sites were observed to cluster around fusion sites [39] and in this work, around a potential fission constriction. Yeast proteins that are reportedly involved in fusion and fission are imported to mitochondria from cytosolic ribosomes [58, 65]. This is therefore consistent with the idea that import sites can redistribute to specific regions of mitochondria [39].

In conclusion, our data provides structural evidence supporting the theory that nuclear-encoded mitochondrial proteins are synthesized locally at the mitochondrial outer membrane. mRNA recruitment to the mitochondrial surface is a key step to sort and polarize translation within the cell [22, 27, 66]. During ongoing translation the distance between the nascent chain and protein translocase is short, increasing the

362 import efficiency [67]. Knowing that protein translocation is much faster than protein
363 translation, protein length may determine if the two processes will occur
364 simultaneously [68]. It is therefore no surprise that the most studied protein thought to
365 be delivered to mitochondria in a co-translational manner is Fum1, with a larger than
366 average molecular weight [69]. Nevertheless, by stalling translation with CHX, we could
367 observed different ribosome populations, including strings of polysomes present on the
368 mitochondrial surface. Thus, at any given time, only a small fraction of ribosomes are
369 seen to interact with the TOM complex, whilst many more could translate
370 mitochondrial proteins from a single mRNA molecule.
371
372 Correct mRNA and protein delivery is likely more challenging with increasing cell
373 volume and a higher demand for timely organization of mitochondrial biogenesis [70].
374 An interesting case was recently reported for the MDI A-kinase anchor protein, present
375 in the mitochondrial outer membrane. MDI recruits a translation stimulator, La-related
376 protein, and promotes mRNA tethering and local protein translation during oogenesis
377 and early embryonic development of *Drosophila melanogaster* [71]. MDI-La-related
378 protein complex formation was crucial for successful hatching and mitochondrial DNA
379 replication, pinpointing the requirement for mRNA localization in efficient
380 mitochondrial biogenesis. Thus, the importance of recruiting RNA molecules coding for
381 mitochondrial proteins to the outer membrane and their localized translation is likely
382 enhanced in specific cell types and developmental stages of higher eukaryotes.

Materials and Methods

Yeast strains and growth conditions

The strains used in this study were derivatives of *Saccharomyces cerevisiae* YPH499 (MAT*a*, *ade2-101, his3-Δ200, leu2-Δ1, ura3-52, trp1-Δ63, lys2-801*) or BY4741 (MAT*a*, *his3Δ1; leu2Δ0; met15Δ0; ura3Δ0*). The YPH499 strains carrying centromeric plasmids that express Tom40, $Tom40_{HA}$ or $Tom22_{HIS}$ were described previously [72-74]. A strain that carried chromosomally integrated $uL13a_{TAP}$ was purchased from GE Dharmacon (Lafayette, CO, USA).

Yeast were grown at 19 – 24 °C on YPGal medium (1% w/v yeast extract, 2% w/v bactopeptone, 2% w/v galactose) with the addition of 0.1% w/v glucose or YPG medium (1% w/v yeast extract, 2% w/v bactopeptone, 3% w/v glycerol) to mid-logarithmic phase. To stabilize ribosomes media were supplemented with 50 µg ml^{-1} of CHX for the final 45 min of the culture as indicated.

Purification of mitochondria and MAR samples

Crude mitochondria were isolated according to a standard procedure [75] and resuspended in sucrose/MOPS (SM) buffer composed of 250 mM sucrose, 10 mM MOPS-KOH (pH 7.2). For crude MAR isolation, solutions were supplemented with 50 µg ml^{-1} CHX and 2 mM $Mg(OAc)_2$. For protein steady-state level analysis, mitochondria were solubilized in Laemmli buffer with 50 mM DTT, denatured at 65 °C for 15 min and analyzed by SDS-PAGE and Western blotting.

For further MAR purification, OptiPrep iodixanol density gradient medium (Sigma-Aldrich, St. Louis, MO, USA) was used. Crude MAR were separated on a step gradient

409 with 10 layers (1 ml volume each) ranging from 0 to 27% v/v of iodixanol in Gradient
410 buffer (10 mM Tris-HCl, 8.75% w/v sorbitol, 2 mM $Mg(OAc)_2$, 50 µg ml^{-1} CHX, pH 7.4) by
411 centrifugation at 80,000 x *g* for 40 min at 4 °C using SW41 Ti rotor (Beckman Coulter
412 Inc., Miami, FL, USA). To analyze the organellar sedimentation profile, each gradient
413 fraction was collected and precipitated with 10% (w/v) trichloroacetic acid (Carl Roth
414 GmbH). The protein pellet was washed with iced-cold acetone, solubilized in Urea
415 Sample buffer (6 M Urea, 125 mM Tris-HCl, 6% SDS, 50mM DTT and 0.01% (w/v)
416 bromophenol blue , pH 6.8) denatured at 37 °C for 15 min and analyzed by SDS-PAGE
417 followed by Western blotting. For cryoET analysis, fractions with the highest
418 mitochondrial content (corresponding to 15% and 21% iodixanol concentrations) were
419 pooled, diluted 10-fold with SM buffer supplemented with 50 µg ml^{-1} CHX and 2 mM
420 $Mg(OAc)_2$ and centrifuged at 22,000 x *g* for 20 min at 4 °C to re-isolate MAR. Pelleted
421 MAR were resuspended in SM buffer as before and used for further analysis.
422
423 **Isolation of high molecular weight membranes**
424 To isolate HMW membranes, yeast cells were harvested, washed with ice-cold water
425 and disrupted in Lysis buffer (20 mM Tris-HCl, 10% w/v glycerol, 100 mM NaCl, 2 mM
426 PMSF, 50 mM iodoacetamide, pH 7.4) with glass beads (425-600 µm, Sigma-Aldrich)
427 using a Cell Disruptor Genie (Scientific Industries, Bohemia, NY, USA) at 2,800 rpm for 7
428 min at 4 °C. To isolate HMW membranes under ribosome stabilizing conditions, Lysis
429 buffer was supplemented with 2 mM $Mg(OAc)_2$ and 50 µg ml^{-1} CHX. Cell debris were
430 removed by centrifugation at 4,000 x *g* for 5 min at 4 °C. HMW membranes were
431 pelleted by centrifugation at 20,000 x *g* for 15 min at 4 °C, washed and resuspended in
432 Lysis buffer. The protein concentration was determined by the Bradford method. To
433 confirm mitochondrial enrichment, the equal amount of control mitochondria and
434 HMW membranes, based on protein concentration, were solubilized in Laemmli buffer

435 containing 50 mM DTT, denatured at 65 °C for 15 min and protein steady-state levels
436 were analyzed by SDS-PAGE and Western blotting.
437
438 **Dissipation of the mitochondrial inner membrane electrochemical potential**
439 Cells were treated with 10 µM CCCP (Sigma-Aldrich) for 0.5 - 3 hours before cell
440 harvesting. Translation was inhibited by addition of 50 µg ml^{-1} CHX prior to cell
441 harvesting and followed by MAR or HMW membranes isolation.
442
443 **Nascent chain release assay**
444 In order to analyze ribosome dissociation from mitochondria upon nascent chain
445 release, 55 µg of crude mitochondria or MAR were suspended in 550 µl of Release
446 buffer (10 mM HEPES, 250 mM sucrose, 80 mM KCl, 5 mM $MgCl_2$, 5 mM methionine, 10
447 mM KH_2PO_4) or SM buffer, both supplemented with 0 - 1.5 M hydroxylamine (Sigma-
448 Aldrich), 3 mM puromycin dihydrochloride (Sigma-Aldrich) or 25 mM EDTA, adjusted to
449 pH 7.4 with HCl) and incubated for 15 min at 30 °C with gentle shaking. Mitochondria
450 were re-isolated by centrifugation at 20,000 x *g*, washed with SM buffer and analyzed
451 by SDS-PAGE followed by Western blotting. To purify MAR after nascent chain release,
452 2 mg of isolated crude MAR were incubated for 15 min at 30 °C in 2 mL of Release
453 buffer with 1.5 M hydroxylamine and separated on 0-27 % iodoxanol gradient.
454
455 **Immuno-affinity purification of $Tom40_{HA}$**
456 MAR (600 µg) or HMW membranes (3 mg) isolated from cells expressing either a wild-
457 type or HA-tagged version of Tom40 were solubilized in Digitonin buffer A (1% w/v
458 digitonin, 20 mM Tris-HCl, 150 mM NaCl, 10% w/v glycerol, 50 mM iodoacetamide, 1
459 mM PMSF, 2 mM $Mg(OAc)_2$, 50 µg ml^{-1} CHX, pH 7.4) for 20 min at 4 °C. After clarifying
460 centrifugation at 20,000 x *g* for 15 min at 4 °C, supernatants were incubated with anti-

HA agarose (Sigma-Aldrich) for 1.5 h at 4 °C. Protein complexes were eluted by incubation with Laemmli buffer with 50 mM DTT. Samples were analyzed by SDS-PAGE and Western blotting.

Immuno-affinity purification of Tom22$_{His}$

1 mg of isolated MAR containing HIS-tagged Tom22 (Tom22$_{HIS}$) were suspended in Buffer B (10 mM MOPS-KOH, 250 mM sucrose, 80 mM KCl, 5 mM $MgCl_2$, 5 mM methionine, 10 mM KH_2PO_4/ K_2HPO_4, pH 7.2) supplemented with 25 mM EDTA in order to disrupt ribosomes. Control samples were mixed with Buffer B without EDTA. After incubation for 20 min at 4 °C, all samples were centrifuged at 20,000 x *g* for 10 min at 4 °C, washed with Buffer B and the pellet solubilized in Digitonin buffer C (1% w/v digitonin, 20 mM Tris-HCl, 100 mM NaCl, 10% w/v glycerol, 50 mM iodoacetamide, 20 mM imidazole, 1 mM PMSF, 2 mM $Mg(OAc)_2$, 50 µg ml^{-1} CHX, pH 7.4) for 20 min at 4 °C. After a clarifying centrifugation at 20,000 x *g* for 15 min at 4 °C, the supernatant was incubated with Ni-NTA agarose (Qiagen, Hilden, Germany) for 1 h at 4 °C. Protein complexes were eluted by incubation with Elution buffer (20 mM Tris-HCl, 100 mM NaCl, 400 mM imidazole, pH 7.4). Eluted proteins were precipitated with StrataClean resin (Agilent Technologies, Santa Clara, CA, USA). The samples were incubated with Laemmli buffer with 50 mM DTT at 65 °C for 15 min and analyzed by SDS-PAGE followed by Western blotting.

Immuno-affinity purification of uL13a$_{TAP}$

uL13a$_{TAP}$ cells were treated with CHX, pelleted and washed with ice-cold water. Yeast cells were resuspended in Lysis buffer supplemented with 2 mM $Mg(OAc)_2$ and 50 µg ml^{-1} CHX, followed by disruption with glass beads using the Cell Disruptor Genie at 2,800 rpm, for 7 min at 4 °C. Cell debris were removed by centrifugation at 20,000 x *g*

for 15 min at 4 °C. The protein concentration of the supernatant (cytoplasmic fraction) was determined by the Bradford method. 3 mg of protein were incubated with 1.5 M hydroxylamine for 30 min at 30 °C with gentle shaking. Samples were cooled on ice and subjected to IgG–Sepharose (GE Healthcare) affinity chromatography for 1 h at 4 °C. The column was washed 3 times with Washing buffer (20 mM Tris-HCl, 150 mM NaCl, 2 mM $Mg(OAc)_2$, 50 µg ml^{-1} CHX, pH 7.4), followed by the elution of protein complexes with Laemmli buffer with 50 mM DTT. Samples were analyzed by SDS-PAGE and Western blotting.

Generation of RNCs and release assay

[^{35}S] methionine labeled Tim9-RNCs were generated as described previously [52]. Radiolabeled RNCs were resuspended in Release buffer supplemented with 1.5 M hydroxylamine and incubated for 30 min at 30 °C with gentle shaking. Reaction mixtures were mixed with Laemmli buffer containing 50 mM iodoacetamide, denatured at 65 °C for 15 min and analyzed by SDS-PAGE followed by autoradiography (Variable Mode Imager Typhoon Trio, GE Healthcare).

Electron cryo-tomography and subtomogram averaging

Mitochondrial samples at a protein concentration of ~5 mg ml^{-1} total mitochondrial protein were mixed 1:1 with 10 nm protein A-gold (Aurion, Wageningen, The Netherlands) as fiducial markers and applied to glow-discharged R2/2 Cu 300 mesh holey carbon coated support grids (Quantifoil, Jena, Germany) by gentle pipetting. Grids were blotted for ~4 s in a humidified atmosphere and plunge-frozen in liquid ethane in a home-made device. Dose-fractionated tomograms (3-8 frames per projection image) were typically collected from +60° to -60° at tilt steps of 2° and 5-8

µm underfocus with a total dose per tomogram of <140$e^-/Å^2$. Data collected at 42,000x (corresponding to a pixel size of 3.3 Å) on the Titan Krios were used for all StA.

Electron cryo-tomography

Tomography was performed either using a Tecnai Polara, Titan Krios (FEI, Hillsboro, USA) or JEM-3200FSC (JEOL, Tokyo, Japan) microscope. All microscopes are equipped with field emission guns operating at 300 keV, K2 Summit direct electron detector cameras (Gatan, Pleasanton, USA) and either a post-column Quantum energy filter operated at a slit width of 20 eV (FEI microscopes) or an in-column energy filter operated with a slit width of 40 eV (JEOL microscope). Dose fractionated data were collected using Digital Micrograph (Gatan) with various pixel sizes (depending on the microscope) per image. Tomograms were aligned using the gold fiducial markers and volumes reconstructed by weighted back-projection using the IMOD software [76]. Contrast was enhanced by non-linear anisotropic diffusion (NAD) filtering in IMOD [77]. Segmentation was performed using AMIRA (FEI).

Subtomogram averaging

For the MAR-M and ER-R populations, two-point coordinates corresponding to the centre of the ribosome and the centre of either the outer mitochondrial or ER-membrane were marked manually in IMOD [76]. Sub-volumes from twice-binned tomograms were then extracted from NAD filtered data and an initial alignment and averaging performed in SPIDER [78]. This average was used as a reference for alignment and refinement using PEET [79]. A full 360° search was performed in Phi (twist around the particle), whereas Theta and Psi (bending in the x-y plane and z angles respectively) covered only +/-90°. 1215 subvolumes were used for the MAR-M structure and 230 subvolumes for the ER-R calculation, using a mask to exclude the

membrane from the alignment. In the final iteration step for the MAR-M average, NAD-filtered tomograms were replaced by unfiltered contrast transfer function (CTF)-corrected data (Fig. 3d). Due to the reduced particle number for the ER-R population, this final step was not performed. Resolution estimates were obtained using conventional 'even/odd' Fourier shell correlation (FSC), applying the 0.5 FSC criterion, using a mask to exclude the membranes from this estimate. In order to visualize the distribution and orientation of the MAR-P population in 3D space, a StA was also calculated. One-point co-ordinates were selected in the centre of each ribosome, and subvolumes extracted for a full angular search in all three directions (Fig. 3e). All NAD-filtered ribosome populations were displayed in AMIRA using the PlaceObjectsInSpace tool (Fig. 3). X-ray data of yeast ribosomes (PDB-4V6I with PDB-3IZD, including a model of the position of eS27^{L}) [63] were docked into comparably NAD-filtered 3D maps of MAR-M or ER-R structures using Chimera (Fig. 5e & f), which was also used to remove low contrast background noise for display using the 'hide dust' tool (UCSF, San Francisco, USA).

Calculation of the number of ribosomes associated with each mitochondrion

In order to calculate the approximate number of ribosomes bound to mitochondria during optimization of sample preparation (Fig. 1a), only side-view ribosomes were counted. This is due to the 'missing wedge' of information in tomography and the difficulty in identifying ribosomes bound to the upper and lower surfaces of mitochondria, especially those that are large and dense (> 500 nm). These values should therefore not be taken as absolute, but rather as a relative comparison between all 4 sample preparation conditions. Sample sizes for side-view ribosomes (Fig. 1a) are taken from 22 mitochondria in total and accumulate as follows: 30 MAR in +$Mg(OAc)_2$, 206 MAR in +$Mg(OAc)_2$ +CHX and 824 MAR in +$Mg(OAc)_2$ +CHX +I. After further data

collection, an accurate absolute value was calculated for MAR-M and MAR-P populations under final stabilizing conditions (+$Mg(OAc)_2$ +CHX +I in Fig. 1a), by selecting only mitochondria in thin ice (< 500 nm) for the analysis, whereby ribosomes could be clearly defined around the entire circumference (Fig. 4b). This was performed for 923 MAR-M and 523 MAR-P data points, combined from 6 mitochondria. Calculation of mitochondrial surface area was performed as previously described [39].

Calculation of ribosome distribution and clustering

The distance between ribosomes, and between ribosomes and CJs, was determined with a MATLAB (Mathworks, California, USA) script as previously described [39]. In order to calculate an accurate value based on coverage of the entire mitochondrial surface, again only mitochondria that demonstrated both side-views and clear upper and lower surface views of ribosomes were included in the analysis. This was performed for 923 MAR-M, combined from 6 mitochondria. Averaged histograms were calculated to depict the mean frequency of occurrence for each minimal distance. To account for the different numbers of ribosomes in each data set, the mean frequency was calculated as a percentage.

Calculation of ribosome distances from membranes

To calculate the distance between MAR-M or ER-R and their respective membranes, the xyz co-ordinates corresponding to the position of the cleft between the 60S and 40S ribosomal subunits and the membrane were extracted and plotted. Again, only side-views of ribosomes were used due to the difficulty in accurately defining both the position of the cleft and the membrane in upper and lower surface views. The cleft was chosen as a reference point as it is a clearly definable feature in individual tomograms.

This accrued 824 data points from 15 tomograms for MAR-P and 140 data points from 11 tomograms for ER-R.

Miscellaneous

Protein concentration was measured by Bradford method using Roti-Quant (Carl Roth GmbH) with bovine serum albumin as a standard. SDS-PAGE was performed according to standard procedures. Protein extracts were examined on 12% and 15% acrylamide gels. Western blot was performed using PVDF membranes (Millipore, Billerica, MA, USA) and specific antisera were used for protein immunodetection. HA-tagged and TAP-tagged proteins were detected by the use of monoclonal anti-HA and PAP Soluble Complex antibodies (Sigma-Aldrich), respectively. Enhanced chemiluminescence signals were detected by X-ray films (Foma Bohemia, Hradec Kralove, Czech Republic), digitalized by Perfection V850 Pro scanner (EPSON, Long Beach, CA, USA) and quantified using ImageQuant TL (GE Healthcare) software. The images were processed using Photoshop CS4 (Adobe Systems, San Jose, CA, USA). The nomenclature of proteins is according to the Saccharomyces Genome Database (SGD). For ribosomal proteins, unified nomenclature was used according to [80].

Acknowledgements

We thank Werner Kühlbrandt for his support, Deryck Mills for excellent maintenance of the EM facility, Inmaculada Mora Espi and Magdalena Dlugolecka for experimental assistance, Sabine Rospert, Paulina Sakowska and Sean Connell for materials and helpful advice and Nikolaus Pfanner, Martin van der Laan and Raffaele Ieva who participated in the published work on TOM-TIM23 supercomplexes shown in Fig 4C. This work was supported by the Max Planck Society, Foundation for Polish Science – Welcome Programme co-financed by the EU within the European Regional

615 Development Fund and National Science Centre, Poland (NCN) grant DEC-
616 2013/11/B/NZ3/00974. P.B. was supported by NCN grant DEC-2013/11/D/NZ1/02294.
617 The authors declare no competing financial interests.

618

619 **Author Contributions**

620 V.A.M.G. and A.C. designed the study. V.A.M.G, P.C. and P.B. performed the
621 experiments and evaluated the data together with A.C. V.A.M.G and P.C. prepared the
622 figures. V.A.M.G., P.C. and A.C wrote the manuscript. All authors commented on the
623 manuscript.

624

625 **Conflict of interest**

626 The authors declare that they have no conflict of interest.

627 **References**

628

629 1. Palade GE (1956) The endoplasmic reticulum. *J Biophys Biochem Cytol* **2**: 85-98

630 2. Adelman MR, Blobel G, Sabatini DD (1973) An improved cell fractionation

631 procedure for the preparation of rat liver membrane-bound ribosomes. *J Cell Biol* **56**:

632 191-205

633 3. Mahamid J, Pfeffer S, Schaffer M, Villa E, Danev R, Cuellar LK, Förster F, Hyman

634 AA, Plitzko JM, Baumeister W (2016) Visualizing the molecular sociology at the HeLa

635 cell nuclear periphery. *Science* **351**: 969-72

636 4. Becker T, Bhushan S, Jarasch A, Armache JP, Funes S, Jossinet F, Gumbart J,

637 Mielke T, Berninghausen O, Schulten K*, et al.* (2009) Structure of monomeric yeast and

638 mammalian Sec61 complexes interacting with the translating ribosome. *Science* **326**:

639 1369-73

640 5. Park E, Rapoport TA (2012) Mechanisms of Sec61/SecY-mediated protein

641 translocation across membranes. *Annu Rev Biophys* **41**: 21-40

642 6. Zhang Y, Berndt U, Gölz H, Tais A, Oellerer S, Wölfle T, Fitzke E, Rospert S

643 (2012) NAC functions as a modulator of SRP during the early steps of protein targeting

644 to the endoplasmic reticulum. *Mol Biol Cell* **23**: 3027-40

645 7. Pfeffer S, Burbaum L, Unverdorben P, Pech M, Chen Y, Zimmermann R,

646 Beckmann R, Förster F (2015) Structure of the native Sec61 protein-conducting channel.

647 *Nat Commun* **6**: 8403

648 8. Elvekrog MM, Walter P (2015) Dynamics of co-translational protein targeting.

649 *Curr Opin Chem Biol* **29**: 79-86

650 9. Sickmann A, Reinders J, Wagner Y, Joppich C, Zahedi R, Meyer HE, Schönfisch B,

651 Perschil I, Chacinska A, Guiard B*, et al.* (2003) The proteome of Saccharomyces

652 cerevisiae mitochondria. *Proc Natl Acad Sci U S A* **100**: 13207-12

653 10. Pfanner N, Wiedemann N, Meisinger C, Lithgow T (2004) Assembling the
654 mitochondrial outer membrane. *Nat Struct Mol Biol* **11**: 1044-8
655 11. Neupert W, Herrmann JM (2007) Translocation of proteins into mitochondria.
656 *Annu Rev Biochem* **76**: 723-49
657 12. Chacinska A, Koehler CM, Milenkovic D, Lithgow T, Pfanner N (2009) Importing
658 mitochondrial proteins: machineries and mechanisms. *Cell* **138**: 628-44
659 13. Mokranjac D, Neupert W (2009) Thirty years of protein translocation into
660 mitochondria: unexpectedly complex and still puzzling. *Biochim Biophys Acta* **1793**: 33-
661 41
662 14. Endo T, Yamano K, Kawano S (2011) Structural insight into the mitochondrial
663 protein import system. *Biochim Biophys Acta* **1808**: 955-70
664 15. Sokol AM, Sztolsztener ME, Wasilewski M, Heinz E, Chacinska A (2014)
665 Mitochondrial protein translocases for survival and wellbeing. *FEBS Lett* **588**: 2484-95
666 16. Schulz C, Schendzielorz A, Rehling P (2015) Unlocking the presequence import
667 pathway. *Trends Cell Biol* **25**: 265-75
668 17. Harmey MA, Hallermayer G, Korb H, Neupert W (1977) Transport of
669 cytoplasmically synthesized proteins into the mitochondria in a cell free system from
670 Neurospora crassa. *Eur J Biochem* **81**: 533-44
671 18. Reid GA, Schatz G (1982) Import of proteins into mitochondria. Yeast cells
672 grown in the presence of carbonyl cyanide m-chlorophenylhydrazone accumulate
673 massive amounts of some mitochondrial precursor polypeptides. *J Biol Chem* **257**:
674 13056-61
675 19. Hoseini H, Pandey S, Jores T, Schmitt A, Franz-Wachtel M, Macek B, Buchner J,
676 Dimmer KS, Rapaport D (2016) The cytosolic cochaperone Sti1 is relevant for
677 mitochondrial biogenesis and morphology. *FEBS J* **283**: 3338-52

678 20. Kellems RE, Allison VF, Butow RA (1975) Cytoplasmic type 80S ribosomes
679 associated with yeast mitochondria. IV. Attachment of ribosomes to the outer
680 membrane of isolated mitochondria. *J Cell Biol* **65**: 1-14
681 21. Crowley KS, Payne RM (1998) Ribosome binding to mitochondria is regulated
682 by GTP and the transit peptide. *J Biol Chem* **273**: 17278-85
683 22. Suissa M, Schatz G (1982) Import of proteins into mitochondria. Translatable
684 mRNAs for imported mitochondrial proteins are present in free as well as
685 mitochondria-bound cytoplasmic polysomes. *J Biol Chem* **257**: 13048-55
686 23. Egea G, Izquierdo JM, Ricart J, San Martín C, Cuezva JM (1997) mRNA encoding
687 the beta-subunit of the mitochondrial F1-ATPase complex is a localized mRNA in rat
688 hepatocytes. *Biochem J* **322 (Pt 2)**: 557-65
689 24. Corral-Debrinski M, Blugeon C, Jacq C (2000) In yeast, the 3' untranslated
690 region or the presequence of ATM1 is required for the exclusive localization of its
691 mRNA to the vicinity of mitochondria. *Mol Cell Biol* **20**: 7881-92
692 25. Marc P, Margeot A, Devaux F, Blugeon C, Corral-Debrinski M, Jacq C (2002)
693 Genome-wide analysis of mRNAs targeted to yeast mitochondria. *EMBO Rep* **3**: 159-64
694 26. Gadir N, Haim-Vilmovsky L, Kraut-Cohen J, Gerst JE (2011) Localization of
695 mRNAs coding for mitochondrial proteins in the yeast Saccharomyces cerevisiae. *RNA*
696 **17**: 1551-65
697 27. Williams CC, Jan CH, Weissman JS (2014) Targeting and plasticity of
698 mitochondrial proteins revealed by proximity-specific ribosome profiling. *Science* **346**:
699 748-51
700 28. Matsumoto S, Uchiumi T, Saito T, Yagi M, Takazaki S, Kanki T, Kang D (2012)
701 Localization of mRNAs encoding human mitochondrial oxidative phosphorylation
702 proteins. *Mitochondrion* **12**: 391-8

703 29. Gehrke S, Wu Z, Klinkenberg M, Sun Y, Auburger G, Guo S, Lu B (2015) PINK1
704 and Parkin control localized translation of respiratory chain component mRNAs on
705 mitochondria outer membrane. *Cell Metab* **21**: 95-108
706 30. Zabezhinsky D, Slobodin B, Rapaport D, Gerst JE (2016) An Essential Role for
707 COPI in mRNA Localization to Mitochondria and Mitochondrial Function. *Cell Rep* **15**:
708 540-9
709 31. Devaux F, Lelandais G, Garcia M, Goussard S, Jacq C (2010) Posttranscriptional
710 control of mitochondrial biogenesis: spatio-temporal regulation of the protein import
711 process. *FEBS Lett* **584**: 4273-9
712 32. Quenault T, Lithgow T, Traven A (2011) PUF proteins: repression, activation and
713 mRNA localization. *Trends Cell Biol* **21**: 104-12
714 33. Funfschilling U, Rospert S (1999) Nascent polypeptide-associated complex
715 stimulates protein import into yeast mitochondria. *Mol Biol Cell* **10**: 3289-99
716 34. George R, Beddoe T, Landl K, Lithgow T (1998) The yeast nascent polypeptide-
717 associated complex initiates protein targeting to mitochondria in vivo. *Proc Natl Acad*
718 *Sci U S A* **95**: 2296-301
719 35. George R, Walsh P, Beddoe T, Lithgow T (2002) The nascent polypeptide-
720 associated complex (NAC) promotes interaction of ribosomes with the mitochondrial
721 surface in vivo. *FEBS Lett* **516**: 213-6
722 36. MacKenzie JA, Payne RM (2004) Ribosomes specifically bind to mammalian
723 mitochondria via protease-sensitive proteins on the outer membrane. *J Biol Chem* **279**:
724 9803-10
725 37. Lesnik C, Cohen Y, Atir-Lande A, Schuldiner M, Arava Y (2014) OM14 is a
726 mitochondrial receptor for cytosolic ribosomes that supports co-translational import
727 into mitochondria. *Nat Commun* **5**: 5711

728 38. Davies KM, Daum B, Gold VA, Mühleip AW, Brandt T, Blum TB, Mills DJ,
729 Kühlbrandt W (2014) Visualization of ATP synthase dimers in mitochondria by electron
730 cryo-tomography. *J Vis Exp*: 51228
731 39. Gold VA, Ieva R, Walter A, Pfanner N, van der Laan M, Kühlbrandt W (2014)
732 Visualizing active membrane protein complexes by electron cryotomography. *Nat*
733 *Commun* **5**: 4129
734 40. Wilson DN (2014) Ribosome-targeting antibiotics and mechanisms of bacterial
735 resistance. *Nat Rev Microbiol* **12**: 35-48
736 41. Obrig TG, Culp WJ, McKeehan WL, Hardesty B (1971) The mechanism by which
737 cycloheximide and related glutarimide antibiotics inhibit peptide synthesis on
738 reticulocyte ribosomes. *J Biol Chem* **246**: 174-81
739 42. Schneider-Poetsch T, Ju J, Eyler DE, Dang Y, Bhat S, Merrick WC, Green R, Shen
740 B, Liu JO (2010) Inhibition of eukaryotic translation elongation by cycloheximide and
741 lactimidomycin. *Nat Chem Biol* **6**: 209-217
742 43. Wiedmann B, Sakai H, Davis TA, Wiedmann M (1994) A protein complex
743 required for signal-sequence-specific sorting and translocation. *Nature* **370**: 434-40
744 44. Raue U, Oellerer S, Rospert S (2007) Association of protein biogenesis factors at
745 the yeast ribosomal tunnel exit is affected by the translational status and nascent
746 polypeptide sequence. *J Biol Chem* **282**: 7809-16
747 45. Ott AK, Locher L, Koch M, Deuerling E (2015) Functional Dissection of the
748 Nascent Polypeptide-Associated Complex in Saccharomyces cerevisiae. *PLoS One* **10**:
749 e0143457
750 46. Kornmann B, Currie E, Collins SR, Schuldiner M, Nunnari J, Weissman JS, Walter
751 P (2009) An ER-mitochondria tethering complex revealed by a synthetic biology screen.
752 *Science* **325**: 477-81

753 47. Wrobel L, Topf U, Bragoszewski P, Wiese S, Sztolsztener ME, Oeljeklaus S,
754 Varabyova A, Lirski M, Chroscicki P, Mroczek S*, et al.* (2015) Mistargeted mitochondrial
755 proteins activate a proteostatic response in the cytosol. *Nature* **524**: 485-8
756 48. Wilson DN, Nierhaus KH (2006) The E-site story: the importance of maintaining
757 two tRNAs on the ribosome during protein synthesis. *Cell Mol Life Sci* **63**: 2725-37
758 49. Garreau de Loubresse N, Prokhorova I, Holtkamp W, Rodnina MV, Yusupova G,
759 Yusupov M (2014) Structural basis for the inhibition of the eukaryotic ribosome. *Nature*
760 **513**: 517-22
761 50. Cao J, Geballe AP (1996) Inhibition of nascent-peptide release at translation
762 termination. *Mol Cell Biol* **16**: 7109-14
763 51. Ziehr DR, Ellis JP, Culviner PH, Cavagnero S (2010) Production of ribosome-
764 released nascent proteins with optimal physical properties. *Anal Chem* **82**: 4637-43
765 52. von der Malsburg K, Müller JM, Bohnert M, Oeljeklaus S, Kwiatkowska P,
766 Becker T, Loniewska-Lwowska A, Wiese S, Rao S, Milenkovic D*, et al.* (2011) Dual role of
767 mitofilin in mitochondrial membrane organization and protein biogenesis. *Dev Cell* **21**:
768 694-707
769 53. Gilmore R, Collins P, Johnson J, Kellaris K, Rapiejko P (1991) Transcription of
770 full-length and truncated mRNA transcripts to study protein translocation across the
771 endoplasmic reticulum. *Methods Cell Biol* **34**: 223-39
772 54. Pfund C, Lopez-Hoyo N, Ziegelhoffer T, Schilke BA, Lopez-Buesa P, Walter WA,
773 Wiedmann M, Craig EA (1998) The molecular chaperone Ssb from Saccharomyces
774 cerevisiae is a component of the ribosome-nascent chain complex. *EMBO J* **17**: 3981-9
775 55. Warner JR, Rich A, Hall CE (1962) Electron Microscope Studies of Ribosomal
776 Clusters Synthesizing Hemoglobin. *Science* **138**: 1399-403
777 56. Brandt F, Carlson LA, Hartl FU, Baumeister W, Grünewald K (2010) The three-
778 dimensional organization of polyribosomes in intact human cells. *Mol Cell* **39**: 560-9

779 57. Pfeffer S, Brandt F, Hrabe T, Lang S, Eibauer M, Zimmermann R, Förster F
780 (2012) Structure and 3D arrangement of endoplasmic reticulum membrane-associated
781 ribosomes. *Structure* **20**: 1508-18
782 58. van der Bliek AM, Shen Q, Kawajiri S (2013) Mechanisms of mitochondrial
783 fission and fusion. *Cold Spring Harb Perspect Biol* **5**
784 59. Körner C, Barrera M, Dukanovic J, Eydt K, Harner M, Rabl R, Vogel F, Rapaport
785 D, Neupert W, Reichert AS (2012) The C-terminal domain of Fcj1 is required for
786 formation of crista junctions and interacts with the TOB/SAM complex in mitochondria.
787 *Mol Biol Cell* **23**: 2143-55
788 60. van der Laan M, Bohnert M, Wiedemann N, Pfanner N (2012) Role of MINOS in
789 mitochondrial membrane architecture and biogenesis. *Trends Cell Biol* **22**: 185-92
790 61. Kozjak-Pavlovic V (2017) The MICOS complex of human mitochondria. *Cell*
791 *Tissue Res* **367**: 83-93
792 62. Bohnert M, Wenz LS, Zerbes RM, Horvath SE, Stroud DA, von der Malsburg K,
793 Müller JM, Oeljeklaus S, Perschil I, Warscheid B*, et al.* (2012) Role of mitochondrial
794 inner membrane organizing system in protein biogenesis of the mitochondrial outer
795 membrane. *Mol Biol Cell* **23**: 3948-56
796 63. Armache JP, Jarasch A, Anger AM, Villa E, Becker T, Bhushan S, Jossinet F,
797 Habeck M, Dindar G, Franckenberg S*, et al.* (2010) Cryo-EM structure and rRNA model
798 of a translating eukaryotic 80S ribosome at 5.5-A resolution. *Proc Natl Acad Sci U S A*
799 **107**: 19748-53
800 64. Dekker PJ, Martin F, Maarse AC, Bömer U, Müller H, Guiard B, Meijer M,
801 Rassow J, Pfanner N (1997) The Tim core complex defines the number of mitochondrial
802 translocation contact sites and can hold arrested preproteins in the absence of matrix
803 Hsp70-Tim44. *EMBO J* **16**: 5408-19

804 65. Hoppins S, Lackner L, Nunnari J (2007) The machines that divide and fuse
805 mitochondria. *Annu Rev Biochem* **76**: 751-80
806 66. Saint-Georges Y, Garcia M, Delaveau T, Jourdren L, Le Crom S, Lemoine S, Tanty
807 V, Devaux F, Jacq C (2008) Yeast mitochondrial biogenesis: a role for the PUF RNA-
808 binding protein Puf3p in mRNA localization. *PLoS One* **3**: e2293
809 67. Fujiki M, Verner K (1993) Coupling of cytosolic protein synthesis and
810 mitochondrial protein import in yeast. Evidence for cotranslational import in vivo. *J Biol*
811 *Chem* **268**: 1914-20
812 68. Sylvestre J, Vialette S, Corral Debrinski M, Jacq C (2003) Long mRNAs coding for
813 yeast mitochondrial proteins of prokaryotic origin preferentially localize to the vicinity
814 of mitochondria. *Genome Biol* **4**: R44
815 69. Yogev O, Karniely S, Pines O (2007) Translation-coupled translocation of yeast
816 fumarase into mitochondria in vivo. *J Biol Chem* **282**: 29222-9
817 70. Zhang Y, Xu H (2016) Translational regulation of mitochondrial biogenesis.
818 *Biochem Soc Trans* **44**: 1717-1724
819 71. Zhang Y, Chen Y, Gucek M, Xu H (2016) The mitochondrial outer membrane
820 protein MDI promotes local protein synthesis and mtDNA replication. *EMBO J* **35**: 1045-
821 57
822 72. Becker T, Wenz LS, Krüger V, Lehmann W, Müller JM, Goroncy L, Zufall N,
823 Lithgow T, Guiard B, Chacinska A*, et al.* (2011) The mitochondrial import protein Mim1
824 promotes biogenesis of multispanning outer membrane proteins. *J Cell Biol* **194**: 387-
825 95
826 73. Meisinger C, Ryan MT, Hill K, Model K, Lim JH, Sickmann A, Müller H, Meyer HE,
827 Wagner R, Pfanner N (2001) Protein import channel of the outer mitochondrial
828 membrane: a highly stable Tom40-Tom22 core structure differentially interacts with
829 preproteins, small tom proteins, and import receptors. *Mol Cell Biol* **21**: 2337-48

74. Wrobel L, Trojanowska A, Sztolsztener ME, Chacinska A (2013) Mitochondrial protein import: Mia40 facilitates Tim22 translocation into the inner membrane of mitochondria. *Mol Biol Cell* **24**: 543-54

75. Meisinger C, Sommer T, Pfanner N (2000) Purification of Saccharomcyes cerevisiae mitochondria devoid of microsomal and cytosolic contaminations. *Anal Biochem* **287**: 339-42

76. Kremer JR, Mastronarde DN, McIntosh JR (1996) Computer visualization of three-dimensional image data using IMOD. *J Struct Biol* **116**: 71-6

77. Frangakis AS, Hegerl R (2001) Noise reduction in electron tomographic reconstructions using nonlinear anisotropic diffusion. *J Struct Biol* **135**: 239-50

78. Frank J, Radermacher M, Penczek P, Zhu J, Li Y, Ladjadj M, Leith A (1996) SPIDER and WEB: processing and visualization of images in 3D electron microscopy and related fields. *J Struct Biol* **116**: 190-9

79. Nicastro D, Schwartz C, Pierson J, Gaudette R, Porter ME, McIntosh JR (2006) The molecular architecture of axonemes revealed by cryoelectron tomography. *Science* **313**: 944-8

80. Ban N, Beckmann R, Cate JH, Dinman JD, Dragon F, Ellis SR, Lafontaine DL, Lindahl L, Liljas A, Lipton JM*, et al.* (2014) A new system for naming ribosomal proteins. *Curr Opin Struct Biol* **24**: 165-9

850 **Figures**

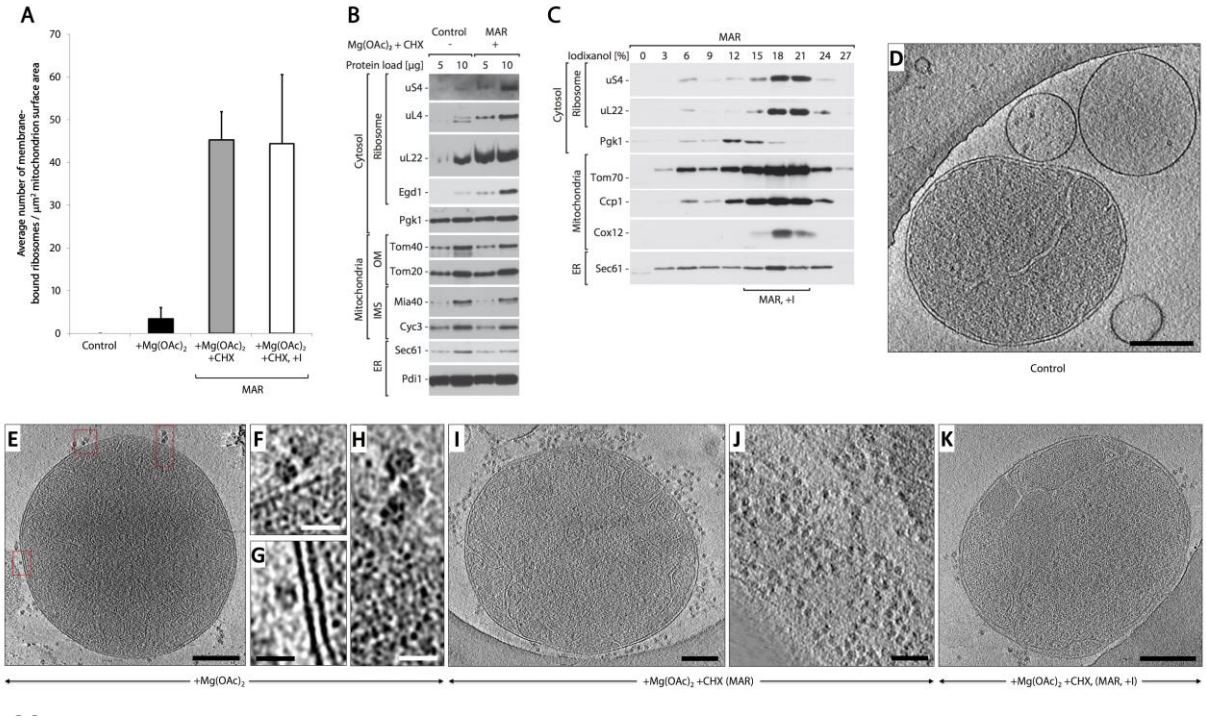

852 **Figure 1 – Mitochondria are enriched with ribosomes after CHX treatment**

853 A Average number of ribosomes bound to mitochondria for Control (-$Mg(OAc)_2$ -
854 CHX), +$Mg(OAc)_2$ only and two +$Mg(OAc)_2$ +CHX (MAR) samples, from a crude isolation
855 and iodixanol purification (+I). Data were collected from 28 mitochondria (1196
856 ribosomes in total + s.e.m).

857 B The steady-state protein levels of isolated crude mitochondria are shown for
858 Control (-$Mg(OAc)_2$ -CHX), and MAR (+$Mg(OAc)_2$ +CHX) samples. Ribosomal proteins co-
859 isolate with mitochondria under ribosome stabilizing conditions (+$Mg(OAc)_2$ +CHX). IMS
860 – intermembrane space, OM – outer membrane.

861 C Fractionation of MAR samples in a 0-27% iodixanol step gradient. Iodixanol
862 gradient purified MAR (MAR, +I) were isolated from 15-21% iodixanol layers. Co-
863 sedimentation of a group of 80S ribosomes with mitochondria indicates their stable
864 interaction.

865 D-K Corresponding example tomographic slices for the data shown in (A). (D)
866 Control (-$Mg(OAc)_2$ -CHX) mitochondria are not associated with ribosomes. Scale bar,
867 0.2 μm. (E) Samples treated with +$Mg(OAc)_2$ only show ribosomes (boxed) bound to
868 mitochondria in a few cases. Scale bar, 0.3 μm. (F-H) Enlargement of the boxes shown
869 in (E). Scale bars, 20 nm. (I) Crude preparation of a MAR (+$Mg(OAc)_2$ +CHX) sample
870 shows many ribosomes bound to mitochondria, but also in (J), a high background of
871 free cytosolic ribosomes that distort accurate analysis. Scale bars, 0.2 μm & 0.1 μm
872 respectively. (K) Analysis of the iodixanol gradient purified MAR sample shows that
873 ribosomes remain stably bound to mitochondria after centrifugation. The background
874 level of free ribosomes and ER-membranes is reduced. Scale bar, 0.2 μm.
875 Data information: In (B-C) samples were analyzed by SDS-PAGE followed by
876 immunodecoration with specific antisera. ER – endoplasmic reticulum.
877

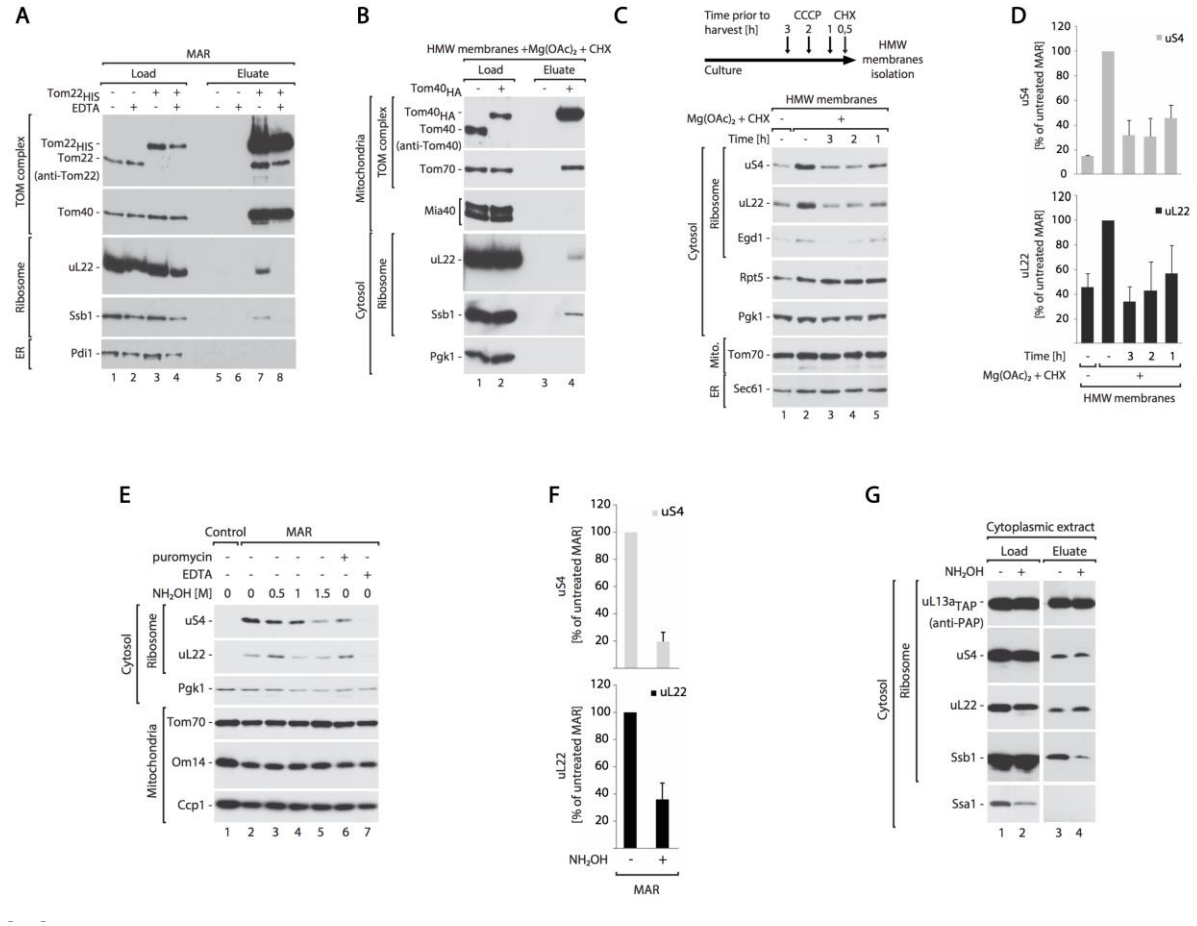

879 **Figure 2 – Cytosolic ribosomes interact with the mitochondrial TOM translocase via**

880 **the nascent chain.**

881 A, B Cytosolic ribosomes co-purify with the TOM complex. (A) Immuno-affinity

882 purification of $Tom22_{HIS}$ from digitonin-solubilized MAR. MAR were pre-treated with 25

883 mM EDTA and washed before solubilization. Load 2%; Eluate 100%. (B) Immuno-affinity

884 purification of $Tom40_{HA}$ from digitonin-solubilized HMW membranes. Load 1%; Eluate

885 100%.

886 C, D Dissipation of the electrochemical inner membrane potential inhibits ribosome

887 recruitment to the mitochondrial surface. (C) The steady-state protein levels of HMW

888 membranes isolated from cells that were either untreated, or treated with 10 µM CCCP

889 for 3, 2 or 1 hour prior to harvesting. Translation was inhibited with 50 µg ml^{-1} CHX for

890 30 min prior to harvesting. For analysis of protein levels after shorter CCCP treatment

891 times see Fig EV2C & D. (D) Quantification of the ribosomal protein levels from samples
892 shown in (C). The protein levels of uS4 and uL22 in MAR were set to 100%. Data are
893 presented as mean + s.e.m, n=3.
894 E-G Ribosomes dissociate from mitochondria upon nascent-chain release. (E)
895 Protein levels in MAR samples upon treatment with nascent-chain releasing agents:
896 hydroxylamine and 3 mM puromycin. 25 mM EDTA was used as reference of ribosome
897 clearance from MAR samples. (F) Quantification of the ribosomal protein levels from
898 untreated MAR and after treatment with 1.5 M hydroxylamine shown in (E, lane 2 and
899 5). The protein levels of uS4 and uL22 in MAR were set to 100%. Data are presented as
900 mean + s.e.m, n=3. (G) TAP-tag affinity purification of the ribosomes from cytoplasmic
901 fraction after hydroxylamine treatment from the uL13a$_{TAP}$ strain. Hydroxylamine causes
902 nascent chain release together with chaperone Ssb1, without affecting 80S ribosome
903 structure. Load 4%; Elution 100%.
904 Data information: In (A-C, E, G) Samples were analyzed by SDS-PAGE and Western
905 blotting using specific antisera.
906

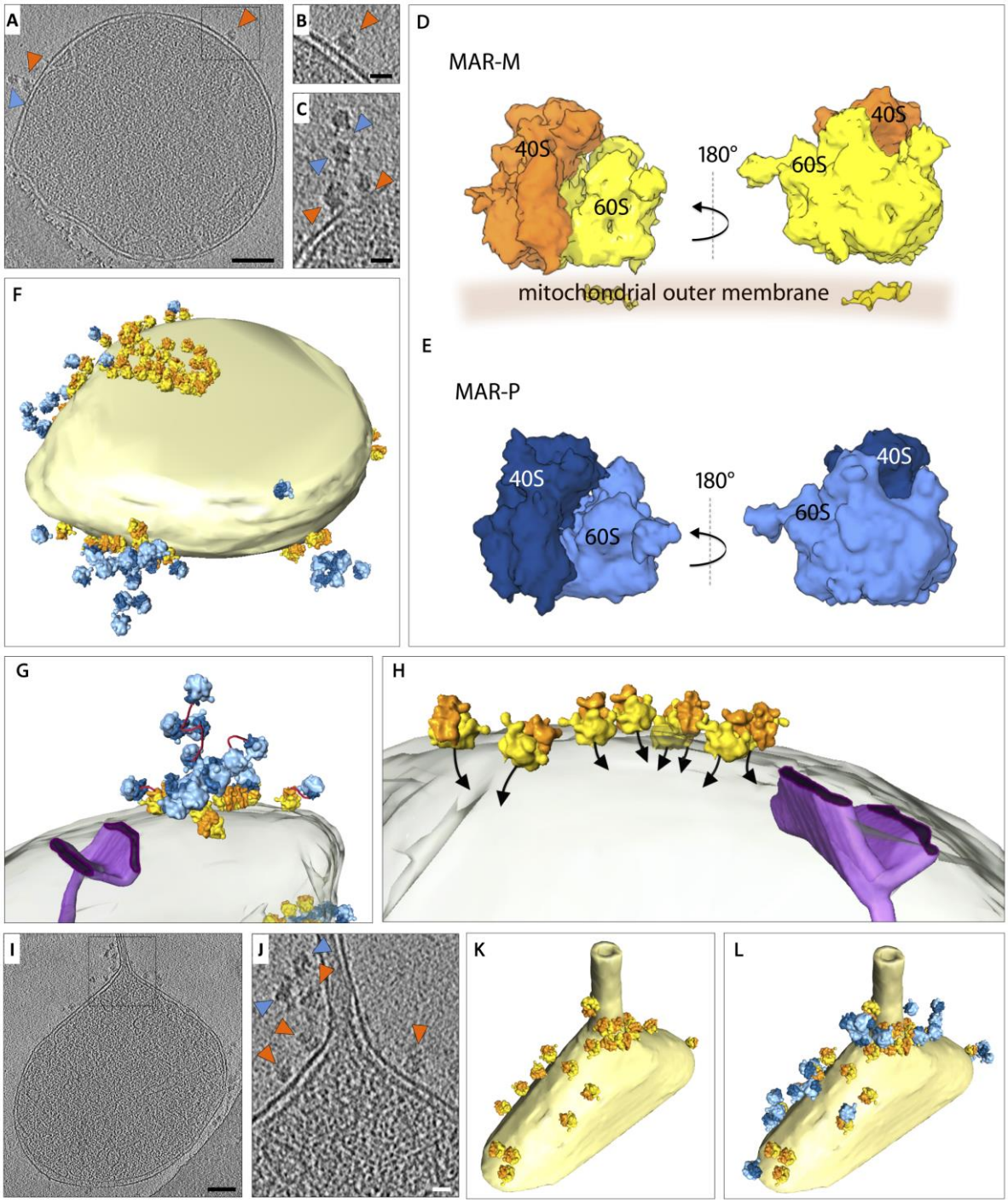

908 **Figure 3 – Ribosomes are oriented for import on the mitochondrial surface**

909 A Tomographic slice showing the location of ribosomes (MAR-M, orange

910 arrowheads; MAR-P, blue arrowheads), associated with a mitochondrion. Scale bar, 0.1

911 μm.

912 B Enlargement of the box shown in (A). Scale bar, 20 nm.

C Tomographic slice showing the arrangement of MAR-M (orange arrowheads) and MAR-P (blue arrowheads). Scale bar, 20 nm.

D StA of the MAR-M population (1215 subvolumes). The 60S subunit (yellow) and 40S subunit (orange) is shown with respect to the position of the mitochondrial membrane.

E StA of the MAR-P population (419 subvolumes). The 60S subunit (light blue) and 40S subunit (dark blue) is shown.

F Surface rendered mitochondrion as shown in (A), showing the distribution of MAR-M and MAR-P groups.

G A MAR-M cluster and associated MAR-P group are shown with respect to the mitochondrial outer membrane (transparent) and a crista junction (purple). The potential path of polysomal mRNA is shown (red).

H Enlargement of a MAR-M cluster shown in (F), depicting the position of the polypeptide exit tunnel (black arrows) with respect to the mitochondrial outer membrane (transparent) and a crista junction (purple).

I Tomographic slice showing the location of ribosomes bound to a mitochondrial outer membrane that has a partially tubular morphology. Scale bar, 0.1 μm.

J Enlargement of the box shown in (I), both the MAR-M (orange arrowheads) and MAR-P (blue arrowheads) distributions are shown. Scale bar, 20 nm.

K Surface rendered mitochondrion as shown in (I), showing the MAR-M distribution and (l) with the MAR-P group included.

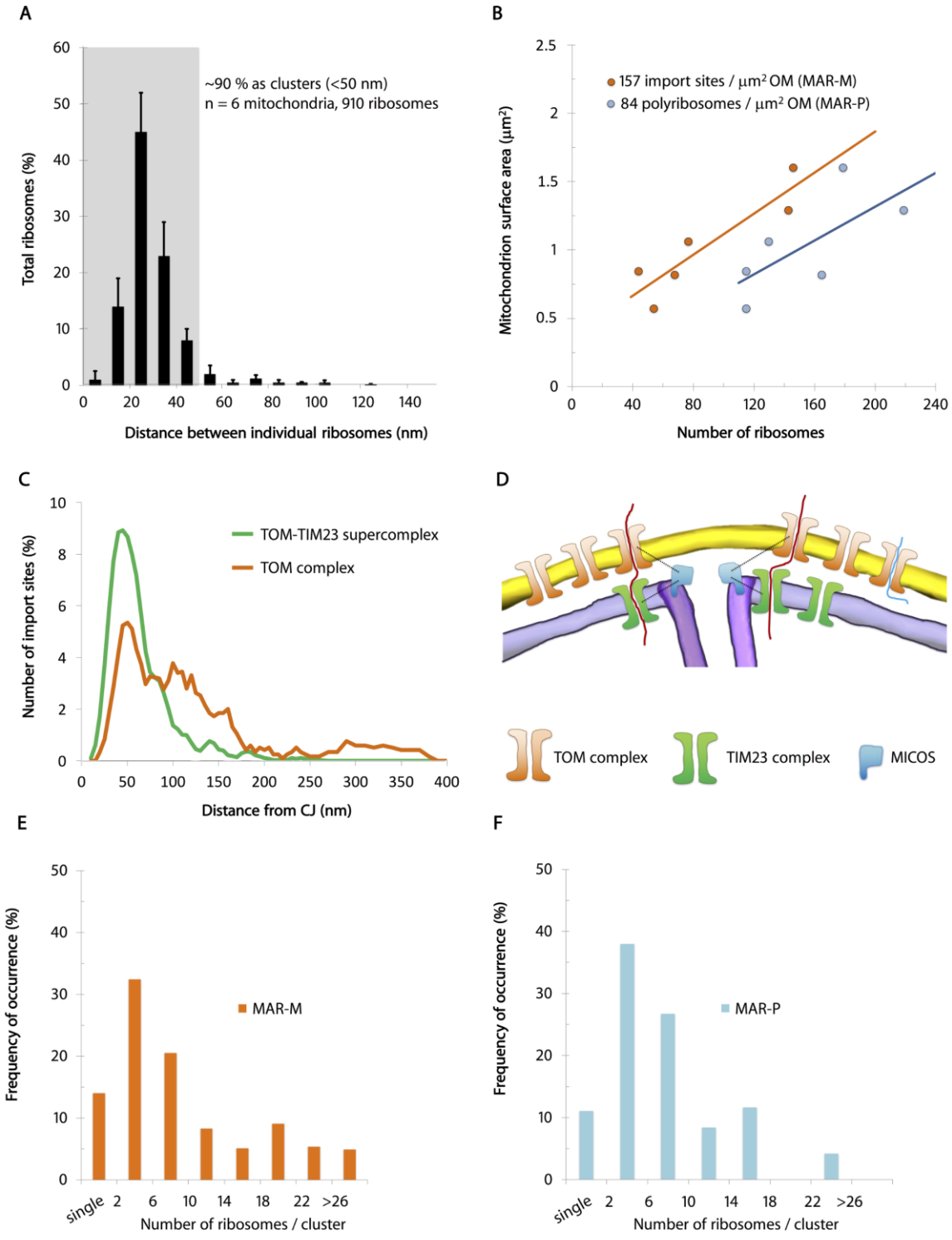

Figure 4 – Ribosomes bind to mitochondria in discrete clusters near CJs

A Histogram showing closest-neighbour distribution distances between individual ribosomes in the MAR-M group, expressed in percent. Error bars indicate the standard deviation of the frequency distribution for each minimal distance.

940 B Scatter plot showing the number of ribosomes (MAR-M, orange; MAR-P, blue)
941 correlated to the surface area of individual mitochondria.
942 C Distribution plot showing the number of import sites (expressed in percent)
943 measured for TOM-TIM23 supercomplexes (green) and ribosome-labelled TOM
944 complexes (orange), correlated to their distance from the nearest CJ. Data are plotted
945 as a moving average in order to reduce the appearance of short-term fluctuations.
946 D Schematic showing the distribution of TOM and TIM23 complexes in the
947 mitochondrial membranes based on data shown in (C). The “mitochondrial contact site
948 and cristae organizing system” (MICOS), responsible for formation and maintenance of
949 the crista junction, is shown with respect to the TOM and TIM23 complexes.
950 E Histogram showing the number of MAR-M per cluster expressed in percent.
951 F Histogram showing the number of MAR-P per cluster expressed in percent.
952 Data information: In (E, F) Data were collected from 6 tomograms in total (923 data
953 points).
954

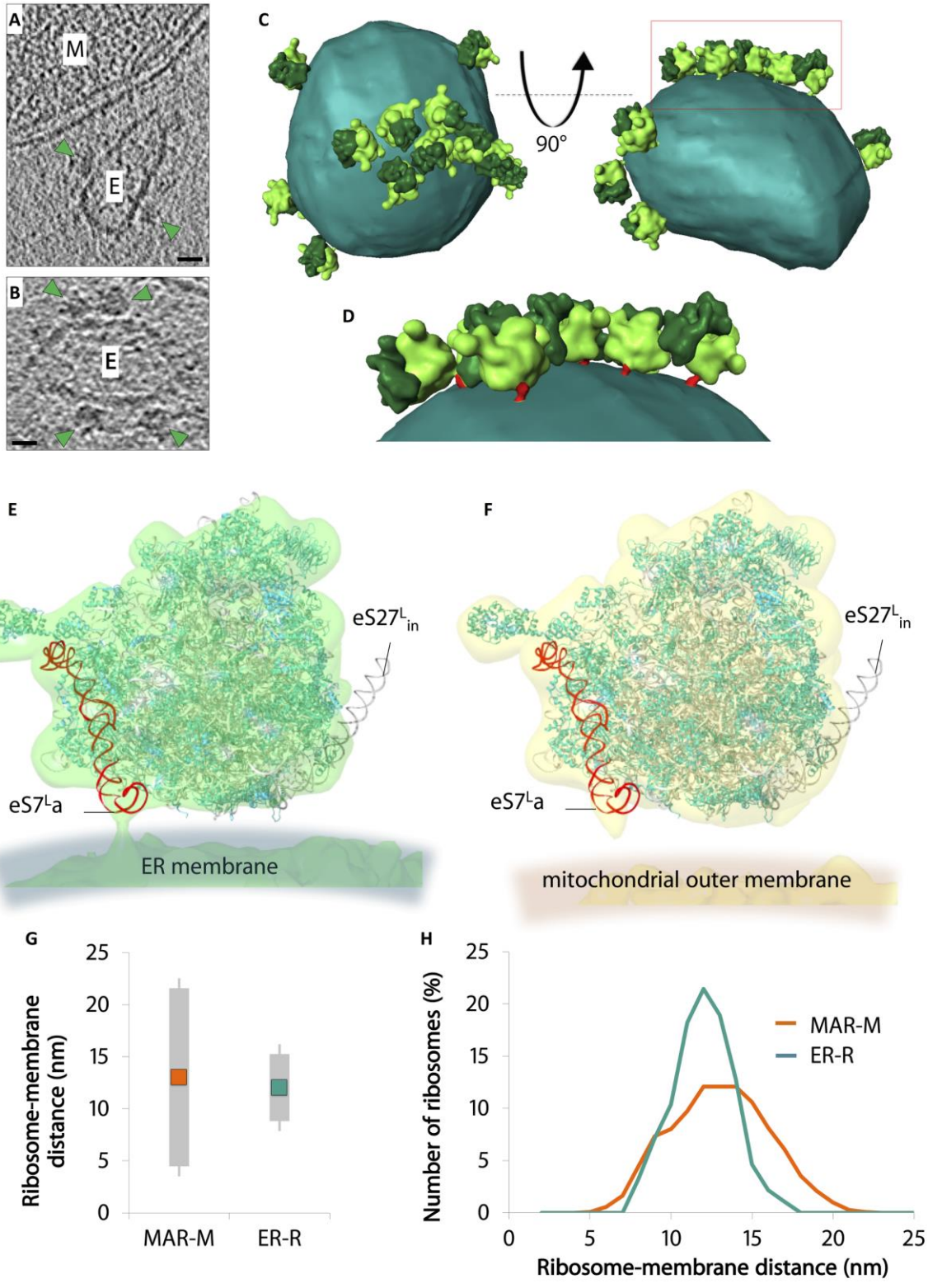

956 **Figure 5 – Ribosomes are tethered to mitochondria through the strength of the**

957 **polypeptide chain interaction**

A, B Reconstructed tomographic slices showing the location of ribosomes (green arrowheads) bound to rough ER membrane vesicles (marked E) that co-purify with mitochondria (marked M). Scale bars, 20 nm.

C Surface rendered rough ER membrane (sea green) showing the position of associated ER-R (60S bright green/ 40S dark green), calculated by StA of 230 subvolumes.

D Enlargement of the red box shown in (c). ER-R attachment to the membrane via ES7^{L}a is also shown (red).

E, F Docked X-ray structures show the positions of ribosomal proteins (teal) and rRNA (grey) in filtered StAs of ER-R (green) and MAR-M (yellow) structures. eS7^{L}a (red) and eS27$^{L}_{in}$ (black) are also shown.

G Graph showing the average distance between MAR-M and the mitochondrial outer membrane (orange) and ER-R and the ER membrane (teal), and the corresponding variance of tethering distances (grey). Calculations are made from the base of the cleft between the 60S and 40S subunits. Data were collected from 15 tomograms (MAR-M) and 11 tomograms (ER-R), accruing 964 data points in total.

H Distribution plot showing the number of ribosomes (expressed in percent) in MAR-M (orange) and ER-R (teal) data sets, correlated to their distance from the membrane. Data are plotted as a moving average in order to reduce the appearance of short-term fluctuations.